

Quantum dynamics of the small-polaron formation in a superconducting analog simulator

Vladimir M. Stojanović^{1,2} and Igor Salom³

¹*Department of Physics, Harvard University, 17 Oxford Street, Cambridge, Massachusetts 02138, USA*

²*Department of Physics, University of Belgrade, Studentski Trg 12, 11158 Belgrade, Serbia*

³*Institute of Physics Belgrade, University of Belgrade, Pregrevica 118, Zemun, Serbia*

(Dated: April 26, 2019)

We propose a scheme for investigating the nonequilibrium aspects of small-polaron physics using an array of superconducting qubits and microwave resonators. This system, which can be realized with transmon- or gatemon qubits, serves as an analog simulator for a lattice model describing a nonlocal coupling of a quantum particle (excitation) to dispersionless phonons. We study its dynamics following an excitation-phonon (qubit-resonator) interaction quench using a numerically-exact approach based on a Chebyshev-moment expansion of the time-evolution operator of the system. We thereby glean heretofore unavailable insights into the process of small-polaron formation resulting from strongly momentum-dependent excitation-phonon interactions, most prominently about its inherent dynamical timescale. To further characterize this complex process, we evaluate the excitation-phonon entanglement entropy and show that initially prepared bare-excitation Bloch states here dynamically evolve into small-polaron states that are close to being maximally entangled. Finally, by computing the dynamical variances of the phonon position- and momentum quadratures we demonstrate a pronounced non-Gaussian character of the latter states, with a strong anti-squeezing in both quadratures.

PACS numbers: 85.25.Cp, 03.67.Ac, 71.38.Ht

I. INTRODUCTION

Recent progress in superconducting (SC) circuits^{1,2} has enabled significant strides in the realm of analog quantum simulation³. An overwhelming majority of proposals for simulating various physical systems using SC circuits is based on arrays of transmon qubits and microwave resonators in state-of-the-art circuit quantum electrodynamics (circuit-QED) setups^{4,5}. Examples include simulators of quantum spin- and spin-boson type systems, interacting fermions/bosons, topological states of matter, to name but a few^{6–8}. In particular, SC simulators of *small-polaron* (SP) models^{9–11} have proven superior to their counterparts based on trapped ions^{12,13}, cold polar molecules^{14,15}, and Rydberg atoms/ions¹⁶. Yet, the existing theoretical proposals for simulating SP physics – not only those based on SC circuits – solely address its static aspects.

The SP concept captures the physical situation often found in narrow-band semiconductors and insulators, where the motion of an itinerant excitation – an excess charge carrier (electron, hole) or an exciton – may get hindered by a potential well resulting from the host-crystal lattice displacements¹⁷. The ensuing SP formation¹⁸, accompanied by the phonon “dressing” of the excitation and an increase in its effective band mass, represents the most striking consequence of strong, short-ranged excitation-phonon (e-ph) coupling¹⁹. Yet, some important issues – e.g, how long it takes for a SP quasiparticle to form following an e-ph interaction quench (i.e., a sudden switching-on of the e-ph interaction in a previously uncoupled system) – remain ill-understood as of this writing^{20,21}. On the theoretical side, this fundamen-

tal issue remains unresolved even in the simplest case of purely local e-ph coupling captured by the time-honored Holstein model^{22–24}. On the experimental side, studies of the dynamics of polaron formation became possible with advances in ultrafast time-resolved spectroscopies, typically yielding formation times of less than a picosecond²⁵.

The compelling need to understand the microscopic mechanisms of charge-carrier transport in complex electronic materials – such as crystalline organic semiconductors^{26,27}, semiconducting counterparts of graphene²⁸, or cuprates^{29,30} – prompted investigations of models with strongly momentum-dependent (nonlocal) e-ph interactions³¹. Such interactions, whose corresponding vertex functions have explicit dependence on both the excitation and phonon quasimomenta, are exemplified by the Peierls-type coupling (also known as Su-Schrieffer-Heeger or off-diagonal coupling³²) that accounts for the dependence of effective excitation hopping amplitudes upon phonon states^{33,34}. Aside from their significance for describing transport properties of materials, such couplings have fundamental importance. Namely, they do not obey the Gerlach-Löwen theorem, a formal result that rules out the existence of non-analytical features in the ground-state-related single-particle properties for certain classes of coupled e-ph models³⁵.

In this paper, motivated by the aforementioned dearth of studies pertaining to the dynamics of SP formation, we explore this complex phenomenon using an analog simulator that consists of SC qubits and microwave resonators. Adjacent qubits are coupled in this system through a coupler circuit that contains three Josephson junctions (JJs). This system, based on transmon qubits,

was proposed in the past by one of us and collaborators for the purpose of simulating static properties of SP's that originate from nonlocal e-ph interactions¹⁰. Apart from transmons, this system can also be realized with semiconductor-nanowire-based gatemon qubits^{36–38}.

We analyze the time-evolution of SP states ensuing from initially prepared bare-excitation Bloch states with different quasimomenta. We do so by combining exact numerical diagonalization of the effective e-ph Hamiltonian of the system and the Chebyshev-propagator method^{39,40} for computing its dynamics. We determine how the SP formation time after an e-ph interaction quench depends on the initial bare-excitation quasimomentum and the e-ph coupling strength. We then further characterize SP formation by evaluating the e-ph entanglement entropy and showing that at the onset of SP regime it reaches values close to those of maximally-entangled states. Besides, we evaluate the dynamical variances of the phonon position- and momentum quadratures in SP states and demonstrate their pronounced non-Gaussian character, with a substantial anti-squeezing in both quadratures. Our findings can be verified in the proposed simulator – once realized – by measuring the photon number and the attendant squeezing in the resonators.

The remainder of this paper is organized as follows. In Sec. II we present the layout of our analog simulator and its underlying Hamiltonian. Sec. II B is set aside for the effective e-ph Hamiltonian of the system, followed by a discussion of typical parameter regimes and the salient features of the SP ground state of the system. In Sec. III we provide a brief outline of the strategy that we employ to study the system dynamics and introduce some relevant timescales in the problem at hand. In Sec. IV we present the obtained results for the SP formation time, as well as those found for the e-ph entanglement entropy and the dynamical variances of the phonon position- and momentum quadratures. We summarize the paper and conclude with some general remarks in Sec. V. Some involved mathematical derivations – as well as a description of basic aspects of the numerical method used and our own implementation thereof – are relegated to the Appendices A – C.

II. SYSTEM AND ITS HAMILTONIAN

A. Layout of the analog simulator

The proposed simulator, depicted in Fig. 1, consists of SC qubits (Q_n) with the energy splitting ε_z , microwave resonators (R_n) with the photon frequency ω_c , and coupler circuits (B_n) with three JJs ($n = 1, \dots, N$). Through the Jordan-Wigner mapping⁴¹ the pseudospin-1/2 degree of freedom of qubits – represented by the operators σ_n – plays the role of a spinless-fermion excitation; photons in the resonators, created by the operators a_n^\dagger , mimic dispersionless phonons. The n -th repeat-

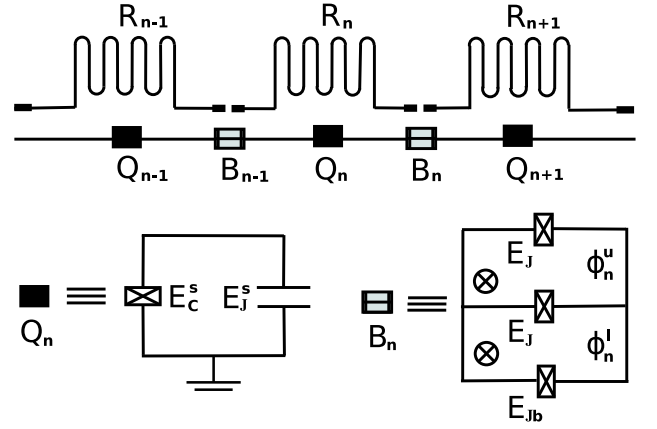


FIG. 1: Schematic diagram of the analog-simulator circuit containing SC qubits Q_n (with charging- and Josephson energies E_C^s and E_J^s , respectively), resonators R_n , and coupler circuits B_n with three Josephson junctions ($n = 1, \dots, N$). ϕ_n^l and ϕ_n^u are total fluxes threading the lower and upper loops of B_n , respectively. Qubit Q_n interacts with its neighbors through circuits B_{n-1} and B_n .

ing unit of this system is described by the Hamiltonian $H_n = H_n^0 + H_n^J$. Its noninteracting part H_n^0 reads

$$H_n^0 = \frac{\varepsilon_z}{2} \sigma_n^z + \hbar \omega_c a_n^\dagger a_n. \quad (1)$$

The Josephson energy of the coupler circuit B_n ⁴² – a generalization of a SQUID loop – is given by

$$H_n^J = - \sum_{i=1}^3 E_J^i \cos \varphi_n^i, \quad (2)$$

where φ_n^i are the respective phase drops on the three JJs and E_J^i their corresponding Josephson energies; we henceforth assume that $E_J^1 = E_J^2 \equiv E_J$ and $E_J^3 = E_{Jb} \neq E_J$.

The qubit- and resonator degrees of freedom are coupled through the flux of the resonator modes that pierces the upper loops of coupler circuits. The Josephson-coupling energy of the latter circuits, as demonstrated in what follows, can be expressed as an XY-type (flip-flop) coupling between adjacent qubits with the coupling strength that dynamically depends on the resonator (i.e., photon) degrees of freedom. As a result, this indirect inductive-coupling mechanism effectively gives rise to a qubit-resonator interaction. Besides, coupler circuits are also driven by a microwave radiation (ac flux) and subject to an external dc flux. The required ac fluxes can be generated by microwave-pumped control wires situated in the vicinity of the respective loops, while the dc flux can be supplied through currents in appropriately placed separate control wires.

Let ϕ_n^u and ϕ_n^l be the respective total magnetic fluxes in the upper and lower loops of B_n (cf. Fig. 1), both expressed in units of $\Phi_0/2\pi$, where $\Phi_0 \equiv hc/(2e)$ is the

flux quantum. The upper-loop flux ϕ_n^u includes the ac-driving contribution $\pi \cos(\omega_0 t)$ and one that stems from the resonator modes, i.e.,

$$\phi_n^u = \pi \cos(\omega_0 t) + \phi_{n,\text{res}}, \quad (3)$$

where $\phi_{n,\text{res}}$ is given by

$$\phi_{n,\text{res}} = \delta\theta[(a_{n+1} + a_{n+1}^\dagger) - (a_n + a_n^\dagger)]. \quad (4)$$

Here $\delta\theta = [2eA_{\text{eff}}/(\hbar d_0 c)] \times (\hbar\omega_c/C_0)^{1/2}$, where A_{eff} is the effective coupling area, C_0 the capacitance of the resonator, and d_0 the effective spacing in the resonator⁴³. The lower-loop flux ϕ_n^l also comprises an ac contribution given by $-(\pi/2) \cos(\omega_0 t)$, with the same frequency as the ac part of ϕ_n^u but a different amplitude. In addition, it includes a dc part ϕ_{dc} – apart from ω_0 the only tunable parameter in the system and its main experimental knob. Thus, ϕ_n^l is given by

$$\phi_n^l = -\frac{\pi}{2} \cos(\omega_0 t) + \phi_{\text{dc}}. \quad (5)$$

It should be stressed that the amplitudes of the two ac-driving terms are chosen in such a way as to ensure that the phase drops φ_n^3 on the bottom JJs do not have an explicit time dependence¹⁰.

The time dependence of the ac-driving terms makes it natural to carry out further analysis in the rotating frame of the drive. While this change of frames leads to a shift in the phonon frequency ($\omega_c \rightarrow \delta\omega \equiv \omega_c - \omega_0$), it also renders the Josephson-coupling term time dependent. Yet, it can easily be shown that this time dependence can be neglected due to its rapidly-oscillating character. The remaining part of that term reads

$$\bar{H}_n^J = -2 \left[t_r - \frac{1}{2} E_J J_1(\pi/2) \phi_{n,\text{res}} \right] \cos(\varphi_n - \varphi_{n+1}). \quad (6)$$

Here φ_n is the gauge-invariant phase variable of the SC island of the n -th qubit¹, $J_n(x)$ are Bessel functions of the first kind, and $t_r = (E_{Jb}/2)(1 + \cos \phi_{\text{dc}})$, where E_{Jb} is chosen to be given by $2E_J J_0(\pi/2)$.

In the regime of relevance for transmon/gatemon qubits ($E_J^s \gg E_C^s$, where E_C^s and E_J^s are the charging- and Josephson energies of a single qubit, respectively) $\cos(\varphi_n - \varphi_{n+1})$ can be expanded up to the second order in $\varphi_n - \varphi_{n+1}$. By switching to the pseudospin operators σ_n , it can be recast (up to an immaterial additive constant) as $\delta\varphi_0^2 [\sigma_n^+ \sigma_{n+1}^- + \sigma_n^- \sigma_{n+1}^+ - (\sigma_n^z + \sigma_{n+1}^z)/2]$. Here $\delta\varphi_0^2 \equiv (2E_C^s/E_J^s)^{1/2}$, hence $\delta\varphi_0^2 \sim 0.15$ for a typical transmon ($E_J^s/E_C^s \sim 100$) and $\delta\varphi_0^2 \sim 0.28$ for a typical gatemon ($E_J^s/E_C^s \sim 25$).

While the original proposal for simulating SP physics with strongly momentum-dependent e-ph interactions (Ref. 10) envisioned the use of transmons – the most widely used type of SC qubits, with superior coherence properties – it is worthwhile to stress that the system under consideration can also be realized with gatemon

qubits^{36–38}. The gatemon is a superconductor-normal-metal-superconductor (SNS) type device where an electrostatic gate depletes carriers in a semiconducting weak-link region. This allows one to tune the energy of its JJ, and in turn control the qubit frequency³⁶. Because it does not require an external-flux control, this gate-voltage-controlled counterpart of the transmon has a reduced dissipation by a resistive control line and is particularly suitable for use in an external magnetic field.

Both types of SC qubits under consideration have some advantages with regard to their use in the proposed analog simulator. On the one hand, the fact that gatemons do not require external-flux control makes them the preferred choice for our present purposes, where the use of external magnetic fluxes is essential (recall Sec. II above). On the other hand, some other aspects – e.g., their larger anharmonicity [see Sec. IV B below] and slightly better coherence properties (for a comparison of coherence properties of various SC-qubit types, see Ref. 2) – favor the use of transmons. For the sake of completeness, it is worthwhile to add that analog simulators of nonlocal e-ph couplings based on other types of SC qubits – e.g., flux qubits that have large anharmonicities – can also be envisaged, as previously proposed for the local-coupling Holstein model¹¹.

B. Effective coupled excitation-phonon Hamiltonian

It is pertinent to switch at this point to the spinless-fermion representation of the qubit (pseudospin-1/2) degrees of freedom. The underlying Jordan-Wigner transformation implies that⁴¹

$$\begin{aligned} \sigma_n^z &\rightarrow 2c_n^\dagger c_n - 1, \\ \sigma_n^+ \sigma_{n+1}^- + \sigma_n^- \sigma_{n+1}^+ &\rightarrow c_n^\dagger c_{n+1} + \text{h.c.} \end{aligned} \quad (7)$$

As a consequence, the noninteracting (free) part H_f of the effective system Hamiltonian – to be denoted as $H_{\text{eff}} = H_f + H_{\text{e-ph}}$ in the following – includes the excitation-hopping- and free-phonon terms

$$H_f = -t_0(\phi_{\text{dc}}) \sum_{n=1}^N (c_n^\dagger c_{n+1} + \text{h.c.}) + \hbar\delta\omega \sum_{n=1}^N a_n^\dagger a_n, \quad (8)$$

where $t_0(\phi_{\text{dc}}) \equiv 2\delta\varphi_0^2 t_r(\phi_{\text{dc}})$ is the ϕ_{dc} -dependent bare-excitation hopping integral. [Note that the σ_n^z terms from H_n^0 and \bar{H}_n^J are omitted as they correspond to a constant band-energy offset for spinless fermions.] Similarly, the interacting part of H_{eff} captures two different mechanisms of nonlocal e-ph interaction and is given by

$$\begin{aligned} H_{\text{e-ph}} &= g\hbar\delta\omega l_0^{-1} \sum_{n=1}^N \left[(c_n^\dagger c_{n+1} + \text{h.c.}) (u_{n+1} - u_n) \right. \\ &\quad \left. - c_n^\dagger c_n (u_{n+1} - u_{n-1}) \right], \end{aligned} \quad (9)$$

where g is the dimensionless coupling strength and $u_n \equiv l_0(a_n + a_n^\dagger)$ the local Einstein-phonon displacement at site n , with l_0 being the phonon zero-point length. The first term of $H_{\text{e-ph}}$ corresponds to the Peierls e-ph coupling mechanism, which captures the lowest-order (linear) dependence of the excitation hopping amplitude between sites n and $n+1$ on the difference $u_{n+1} - u_n$ of the respective phonon displacements^{34,44}. The other one is the breathing-mode term³⁰, a density-displacement-type mechanism which accounts for the antisymmetric coupling of the excitation density $c_n^\dagger c_n$ at site n with the phonon displacements on the adjacent sites $n \pm 1$. In other words, it captures a nonlocal phonon-induced modulation of the excitation's on-site energy (by contrast to Holstein coupling which describes the local phonon-induced modulation of the same energy).

By transforming the e-ph coupling Hamiltonian to its generic momentum-space form

$$H_{\text{e-ph}} = N^{-1/2} \sum_{k,q} \gamma_{\text{e-ph}}(k,q) c_{k+q}^\dagger c_k (a_{-q}^\dagger + a_q), \quad (10)$$

it is straightforward to verify that its corresponding vertex function is given by

$$\gamma_{\text{e-ph}}(k,q) = 2ig\hbar\delta\omega [\sin k + \sin q - \sin(k+q)], \quad (11)$$

where quasimomenta are expressed in units of the inverse lattice period. Because this vertex function depends on both the excitation (k) and phonon (q) quasimomenta the Hamiltonian H_{eff} does not belong to the realm of validity of the Gerlach-Löwen theorem³⁵. As demonstrated in Ref. 10 its ground state displays a level-crossing-type sharp transition at a critical value of the effective coupling strength $\lambda_{\text{eff}} \equiv 2g^2 \hbar\delta\omega/t_0$. While for $\lambda_{\text{eff}} < \lambda_{\text{eff}}^c$ the ground state is the (non-degenerate) $K = 0$ eigenvalue of the total quasimomentum operator

$$K_{\text{tot}} = \sum_k k c_k^\dagger c_k + \sum_q q a_q^\dagger a_q, \quad (12)$$

for $\lambda_{\text{eff}} \geq \lambda_{\text{eff}}^c$ it is twofold-degenerate and corresponds to $K = \pm K_{\text{gs}}$ (where $K_{\text{gs}} \neq 0$ and saturates at $\pi/2$ for sufficiently large λ_{eff}). In this regime the single-particle dispersion corresponding to the SP Bloch band has mutually symmetric minima at two nonzero quasimomenta, which are here incommensurate with the period of the underlying lattice, a rare occurrence in other physical systems⁴⁵.

Aside from a non-analyticity in the ground-state energy of the system, the aforementioned sharp transition is manifested by analogous features in the ground-state quasiparticle residue (spectral weight) $Z_{\text{gs}} \equiv Z_{k=K_{\text{gs}}}$, where $Z_k \equiv |\langle \Psi_k | \psi_k \rangle|^2$ is the module squared of the overlap between the bare-excitation Bloch state

$$|\Psi_k\rangle = c_k^\dagger |0\rangle_{\text{e}} \otimes |0\rangle_{\text{ph}} \quad (13)$$

and the (dressed) Bloch state $|\psi_k\rangle$ of the coupled e-ph system corresponding to the same quasimomentum

($K = k$). [Note that $|0\rangle_{\text{e}}$ and $|0\rangle_{\text{ph}}$ on the right-hand-side (RHS) of the last equation stand for the excitation- and phonon vacuum states, respectively.] Another quantity characterizing the SP ground state, which shows a non-analyticity at $\lambda_{\text{eff}} = \lambda_{\text{eff}}^c$, is the phonon-number expectation value in the ground state $|\psi_{\text{gs}}\rangle \equiv |\psi_{K=K_{\text{gs}}}\rangle$:

$$\bar{N}_{\text{ph}} = \langle \psi_{\text{gs}} | \sum_{n=1}^N a_n^\dagger a_n | \psi_{\text{gs}} \rangle. \quad (14)$$

The system at hand has another peculiar property – namely, it is straightforward to demonstrate that the $k = 0$ bare-excitation Bloch state $|\Psi_{k=0}\rangle$ [cf. Eq. (13)] is an eigenstate of H_{eff} for an arbitrary λ_{eff} , a direct consequence of the fact that the e-ph vertex function [cf. Eq. (11)] has the property that $\gamma_{\text{e-ph}}(k = 0, q) = 0$ for any q . In particular, for $\lambda_{\text{eff}} < \lambda_{\text{eff}}^c$ this state represents the ground state of H_{eff} .

The relation between the dimensionless coupling strength g and the system-specific parameters reads

$$g\hbar\delta\omega = \delta\varphi_0^2 E_J J_1(\pi/2) \delta\theta. \quad (15)$$

It is worthwhile to notice that g does not depend on the tunable system parameters (ω_0 , ϕ_{dc}) and we specify it by fixing the product of $\delta\varphi_0^2$ and E_J on the RHS of the last equation: $\delta\varphi_0^2 E_J / 2\pi\hbar = 100$ GHz. Given that the typical magnitude of $\delta\varphi_0^2$ is twice as large for gatemons compared to transmons, in a transmon-based realization of this system E_J should be taken twice as large to retain the same coupling strength and make further discussion completely general. Unlike g , λ_{eff} inherits its dependence on ϕ_{dc} from t_0 and is therefore externally tunable:

$$\lambda_{\text{eff}}(\phi_{\text{dc}}) = g \frac{J_1(\pi/2) \delta\theta}{J_0(\pi/2) (1 + \cos \phi_{\text{dc}})}. \quad (16)$$

For a typical resonator $\delta\theta \sim 3.5 \times 10^{-3}$. Likewise, for $\delta\omega$ we take $\delta\omega/2\pi = 200 - 300$ MHz. Consequently, for $\delta\omega/2\pi = 200$ MHz (300 MHz) we obtain $\lambda_{\text{eff}}^c \approx 0.83$ (0.72).

III. DYNAMICS OF THE SMALL-POLARON FORMATION

A. Interaction quench and initial-state preparation

We study the system dynamics after an e-ph (qubit-resonator) interaction quench at $t = 0$, assuming that the system was initially prepared in the bare-excitation Bloch state $|\Psi_{k=k_0}\rangle$ with quasimomentum k_0 . Given that an abrupt change from a bare excitation to a heavily-dressed one here takes place for $\lambda_{\text{eff}} = \lambda_{\text{eff}}^c$, a variation of ϕ_{dc} from slightly below its critical value to slightly above it is equivalent to an interaction quench in this system.

The initial bare-excitation states can be prepared using a general protocol based on an external driving and

the Rabi coupling between the vacuum state and the desired Bloch state⁹. The corresponding preparation time is given by $\tau_{\text{prep}} = \pi\hbar/(2\beta_p)$, where β_p is the microwave-pumping amplitude. [Note that an analogous result holds in the case of preparing dressed Bloch states – e.g., a SP ground state – except that in that case the last expression for τ_{prep} requires another multiplicative factor of Z_{gs}^{-1} .] For a typical pumping amplitude $\beta_p/(2\pi\hbar) = 10$ MHz, we obtain $\tau_{\text{prep}} = 25$ ns, which is a three orders of magnitude shorter time than currently achievable decoherence times T_2 of the relevant classes of SC qubits².

B. Relevant quantities and timescales

In accordance with the discrete translational symmetry of the system under consideration, its effective Hamiltonian commutes with the total quasimomentum operator [cf. Eq. (12)], i.e., $[H_{\text{eff}}, K_{\text{tot}}] = 0$. Therefore, the system evolves within the eigensubspace of H_{eff} that corresponds to the eigenvalue $K = k_0$ of K_{tot} . We compute its state $|\psi(t)\rangle$ at time t for a simulator with $N = 9$ qubits by combining Lanczos-type exact diagonalization⁴⁶ of H_{eff} in a symmetry-adapted basis of the truncated Hilbert space of the system (for details, see Appendix A) and the Chebyshev-propagator method^{39,40}. The latter relies on expansions of time-evolution operators into finite series of Chebyshev polynomials of the first kind (for general details of this approach and our numerical implementation thereof, see Appendix C).

The knowledge of the state $|\psi(t)\rangle$ of the system at time t allows us to evaluate quantities characterizing the ensuing polaronic character of the dressed excitation. One such quantity is the probability for the system to remain in the initial state $|\Psi_{k=k_0}\rangle$ at time t , given by

$$P_{k_0}(t) = |\langle\psi(t)|\Psi_{k=k_0}\rangle|^2. \quad (17)$$

This quantity, more precisely the matrix element $\langle\psi(t)|\Psi_{k=k_0}\rangle$, is closely related (up to a Fourier transform to the frequency domain) to the momentum-frequency resolved spectral function, a dynamical response function that can be extracted in systems of the present type using a generalization of the Ramsey interference protocol¹⁰. Another relevant quantity is the expected total phonon number:

$$n_{\text{ph}}(t) = \langle\psi(t)| \sum_{n=1}^N a_n^\dagger a_n |\psi(t)\rangle. \quad (18)$$

This observable provides a direct quantitative characterization of the dynamical dressing of an excitation by virtual phonons. In our analog simulator, $n_{\text{ph}}(t)$ is amenable to measurement by extracting the photon number on the resonators (for details, see Sec. IV B below).

It is judicious to express the evolution time in units of a timescale closely related to the bare-excitation hopping amplitude $t_0(\phi_{\text{dc}})$. Because the latter here depends on the experimental knob ϕ_{dc} by design, we choose this

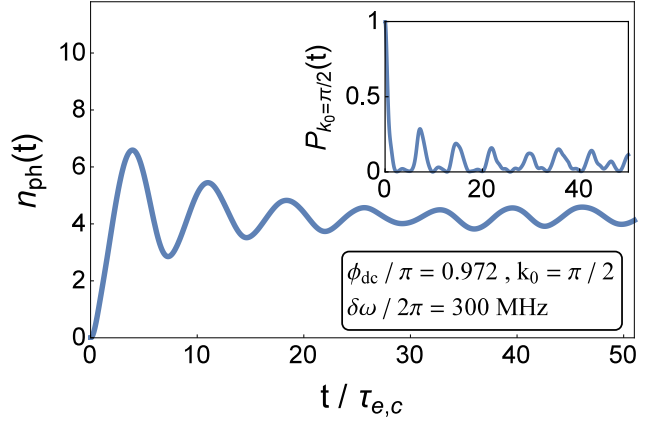


FIG. 2: (Color online) Expected phonon number after an e-ph interaction quench at $t = 0$ for $k_0 = \pi/2$. Inset: the probability to remain in the initial bare-excitation Bloch state.

timescale to be set by the critical value $\phi_{\text{dc}}^c = 0.972\pi$ of ϕ_{dc} for $\delta\omega/2\pi = 300$ MHz. Thus, the chosen characteristic timescale is $\tau_{e,c} \equiv \hbar/t_0(\phi_{\text{dc}}^c) \approx 0.44$ ns.

One of the most important characteristics of the SP formation process – yet often elusive in solid-state systems exhibiting polaronic behavior²⁵ – is its associated dynamical timescale τ_{sp} . It is pertinent to define it as the time at which the phonon dressing (i.e., the phonon-number expectation value) of an initially bare excitation becomes equal to that of the corresponding SP ground state. In other words, τ_{sp} is defined by the condition

$$n_{\text{ph}}(t = \tau_{\text{sp}}) = \bar{N}_{\text{ph}}, \quad (19)$$

where \bar{N}_{ph} was defined in Eq. (14) above. This ground-state phonon number is in the range $3.9 - 5.1$ ($1.8 - 2$) for $\delta\omega/2\pi = 200$ MHz (300 MHz).

IV. RESULTS AND DISCUSSION

A. Time dependence of n_{ph} and $P_{k_0=\pi/2}$

Typical results of our numerical calculations of $n_{\text{ph}}(t)$ and $P_{k_0=\pi/2}(t)$ are presented in Fig. 2. They reflect the fact that the system was initially prepared in the $|\Psi_{k_0=\pi/2}\rangle$ state, which is not an eigenstate of the system Hamiltonian H_{eff} after the quench. In fact, for the concrete choice of parameter values used, this state is a superposition of a multitude of eigenstates of this Hamiltonian, among which the SP ground state with $K_{\text{gs}} = \pi/2$ has a weight of only around 0.16. This explains the presence of dynamical recurrences at later times, i.e., a complex oscillatory behavior resulting from the interference of the quantum evolutions of all these eigenstates.

It is instructive to add, for completeness, that our ground-state calculations show that for $\lambda_{\text{eff}} = \lambda_{\text{eff}}^c$ – i.e., at the onset of strong-coupling regime in the system under consideration – there are 3 discrete states (at each K)

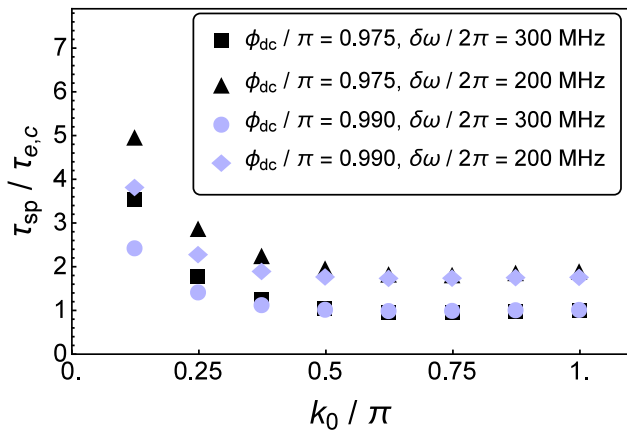


FIG. 3: (Color online) SP formation time τ_{sp} for varying initial bare-excitation quasimomenta k_0 within the Brillouin zone and different choices of values for ϕ_{dc} and $\delta\omega$.

below the one-phonon continuum, while for a larger λ_{eff} one can find up to 5 such states. As a reminder, the one-phonon continuum in a coupled e-ph system with gapped (optical-like) phonon modes – such as, e.g., Einstein-like phonons in the system at hand – originates from the onset of the inelastic-scattering threshold at the energy $E_{gs} + \hbar\omega_{ph}$ (the minimal energy that a dressed excitation ought to have in order to be able to emit a phonon), where E_{gs} is the ground-state energy of the coupled system and $\hbar\omega_{ph}$ the energy of one phonon (in our simulator $\omega_{ph} \rightarrow \delta\omega$)¹⁹. The width of this continuum equals the width of the resulting SP Bloch band. Importantly, the discrete (bound) states below the one-phonon continuum feature as the coherent part, i.e., sharp peaks in the momentum-frequency resolved spectral function¹⁰. While some details of the dynamics certainly depend on the concrete form of e-ph coupling involved, the increasing number of such discrete (split-off from the continuum) states upon increasing coupling strength results in more complex system dynamics.

B. Small-polaron formation time

The dependence of the SP formation time τ_{sp} on the initial bare-excitation quasimomentum k_0 is illustrated in Fig. 3 (for symmetry-related reasons, it suffices to consider only quasimomenta in one half of the Brillouin zone, i.e., for $0 \leq k_0 \leq \pi$). τ_{sp} clearly shows an up-turn for small k_0 , consistent with the fact that it ought to diverge ($\tau_{sp} \rightarrow \infty$) as $k_0 \rightarrow 0$ because the $k_0 = 0$ bare-excitation Bloch state is an exact eigenstate of H_{eff} . Another important feature that can be inferred from the obtained results is that τ_{sp} depends rather weakly on k_0 for $\pi/2 \leq k_0 \leq \pi$. This can be contrasted with the Holstein-polaron case²⁰, where the analogous dynamical timescale strongly depends on the initial bare-excitation quasimomentum.

The obtained dependence of τ_{sp} on the effective coupling strength λ_{eff} is displayed in Fig. 4. While it may seem surprising that τ_{sp} saturates for λ_{eff} above a threshold value, this actually mimics the behavior of the SP indicators (quasiparticle residue, average phonon number) in the ground state. In that case a regime of saturation also sets in for λ_{eff} slightly above its critical value at which a nonanalyticity occurs in all ground-state-related quantities¹⁰. Such a behavior is in stark contrast with that of the momentum-independent Holstein coupling, for which the same quantities change monotonously with the coupling strength.

The variation of the SP formation time – defined by the condition in Eq. (19) – with the effective coupling strength λ_{eff} (shown in Fig. 4) results from two competing tendencies. Namely, with increasing λ_{eff} phonon dressing of an initially bare excitation becomes faster. However, the average ground-state phonon number \bar{N}_{ph} also becomes larger. In Ref. 20, where the dynamics of the Holstein-polaron formation were investigated, a regime was observed where the formation time grows with λ_{eff} (for weak coupling, i.e., small λ_{eff}) and the one where it decreases (strong coupling, i.e., large λ_{eff}). Despite completely different type of e-ph interaction in the system at hand, we also find such regimes. For our typical system parameters, the case with $\delta\omega/2\pi = 200$ MHz [cf. Fig. 4] corresponds to the latter regime, while the case with $\delta\omega/2\pi = 300$ MHz (results not shown here) is characterized by a slow growth of τ_{sp} with increasing λ_{eff} .

The obtained SP formation times $\tau_{sp} \sim (1 - 10) \tau_{e,c}$ justify *a posteriori* our choice of $\tau_{e,c}$ as the characteristic timescale for the system dynamics. These times are of the order of a few nanoseconds and can be verified in this system through photon-number measurements. This is done by adding an ancilla qubit (far-detuned from the resonator modes), which couples – but exclusively during the measurement itself – to a resonator⁹. The photon number on that resonator can then be ex-

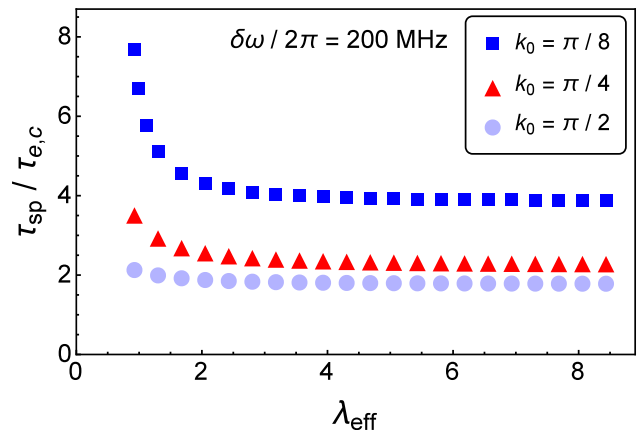


FIG. 4: (Color online) Dependence of the SP formation time τ_{sp} on the effective coupling strength λ_{eff} , shown for $\delta\omega/2\pi = 200$ MHz and different initial quasimomenta k_0 .

tracted by means of a standard quantum non-demolition-measurement readout, which is effectively carried out by measuring the transition frequency of the qubit⁴⁷. The total photon number can then be obtained by adding up those found on individual resonators.

An important issue to address in the context of measuring the photon states in the resonators is the one pertaining to the anharmonicity $\alpha \equiv E_{12} - E_{01}$ of SC qubits, where E_{ij} is the energy difference between states j and i of a single qubit. The anharmonicity determines the minimal pulse duration $t_p \sim \hbar/|\alpha|$ required to avoid leakage into noncomputational single-qubit states. For instance, for a typical transmon with a negative anharmonicity of around 200 MHz, even microwave pulses with durations on the scale of a few nanoseconds are known to be sufficiently frequency selective that one can neglect leakage into higher excited energy levels of the transmon and effectively treat it as a two-level system⁵. For gatemon, whose anharmonicity is slightly smaller than that of transmons³⁸, similar measurements should also be possible for all but the very shortest SP formation times found.

C. Dynamical variances of the phonon position- and momentum quadratures

It is plausible to expect that nonlocal e-ph correlations in this system are reflected through fluctuations within the phonon subsystem, which can be observed via microwave photons in the resonators. To this end, we consider the phonon position- and momentum quadratures at an arbitrary – say r -th – site (in our system represented by the photon mode on the r -th resonator), defined by the operators $x_r \equiv (a_r + a_r^\dagger)/\sqrt{2}$ and $p_r \equiv -i(a_r - a_r^\dagger)/\sqrt{2}$, respectively. We compute their respective dynamical variances $S_x(t)$ and $S_p(t)$, given by

$$\begin{aligned} S_x(t) &= \langle \psi(t) | x_r^2 | \psi(t) \rangle - \langle \psi(t) | x_r | \psi(t) \rangle^2, \\ S_p(t) &= \langle \psi(t) | p_r^2 | \psi(t) \rangle - \langle \psi(t) | p_r | \psi(t) \rangle^2. \end{aligned} \quad (20)$$

[Note that, owing to the discrete translational symmetry of the system, the latter quantities should not depend on r .] The explicit expressions for these variances in our chosen symmetry-adapted basis are provided in Sec. B).

Our numerical evaluation of these dynamical variances shows that S_x dominates over S_p at all times. For instance, in the weakest-coupling case that yields SP ground state in the system at hand – with $\delta\omega/2\pi = 300$ MHz, and $\phi_{dc} = 0.972 \pi$ (shown in Fig. 5, which corresponds to $k_0 = \pi/2$) – one finds the maximum of $S_x(t)$ to be around 12. The corresponding anti-squeezing is as large as 13.8 dB.

What can be inferred from Fig. 5 is that the product $S_x(t) \times S_p(t)$ of the two dynamical quadrature variances is consistently much larger than $1/4$, which illustrates a pronounced non-Gaussian character of fluctuations within the phonon subsystem. This can be ascribed

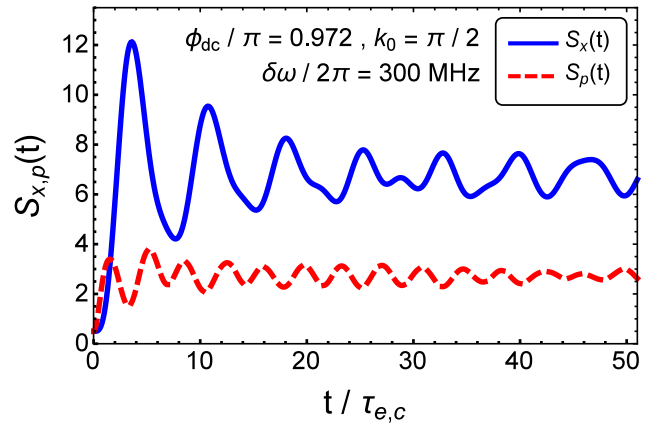


FIG. 5: (Color online) Typical time-dependence of the dynamical variances $S_x(t)$ and $S_p(t)$. The parameter values are indicated in the plot.

to the nonlocal character of e-ph interaction in this system, with its attendant retardation effects³².

D. Dynamics of the excitation-phonon entanglement buildup after the quench

It is worthwhile to complement our discussion of the dynamics of SP formation by evaluating the corresponding e-ph entanglement entropy. This quantity proved to be very useful in characterizing ground-state properties of SPs – most prominently the onset of sharp SP transitions at a critical e-ph coupling strength – in models with strongly momentum-dependent e-ph interactions³⁴. This motivates us to use the same quantity in our present investigation of the SP formation dynamics.

Given that the initial bare-excitation states are of simple-product (separable) character, the e-ph entanglement entropy starts its growth from zero at $t = 0$. The density matrix of our composite (bipartite) e-ph system at time t is given by

$$\rho_{\text{e-ph}}(t) = |\psi(t)\rangle\langle\psi(t)|. \quad (21)$$

The reduced (excitation) density matrix, which has the dimension $N \times N$, is obtained by tracing $\rho_{\text{e-ph}}(t)$ over the phonon basis:

$$\rho_e(t) = \text{Tr}_{\text{ph}}[\rho_{\text{e-ph}}(t)]. \quad (22)$$

The corresponding e-ph entanglement entropy is defined in terms of this last reduced density matrix as

$$S_E(t) = -\text{Tr}_e[\rho_e(t) \ln \rho_e(t)]. \quad (23)$$

The matrix elements of $\rho_e(t)$ are computed using Eq. (B25) [for a detailed derivation of those matrix elements, see Appendix B 2]. The e-ph entanglement entropy in Eq. (23) can equivalently be expressed in terms

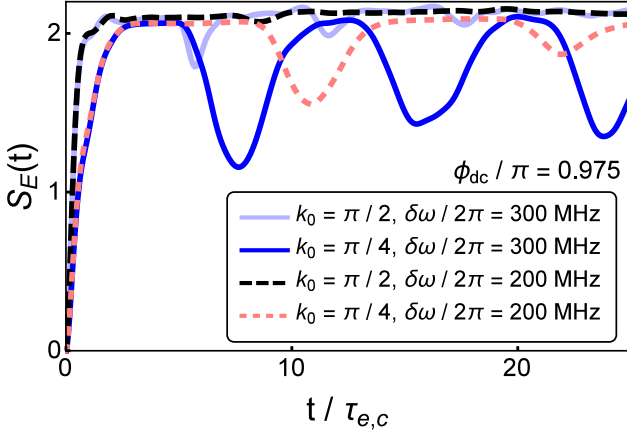


FIG. 6: (Color online) Time-dependence of the e-ph entanglement entropy for $\phi_{dc} = 0.975\pi$ and different choices of values for k_0 and $\delta\omega$.

of the eigenvalues $\xi_n(t)$ ($n = 1, \dots, N$) of $\rho_e(t)$ (note that $\xi_n > 0$ and $\sum_{n=1}^N \xi_n = 1$):

$$S_E(t) = - \sum_{n=1}^N \xi_n(t) \ln \xi_n(t). \quad (24)$$

Generally speaking, the maximal value that can be reached by this quantity is

$$S_{\text{max-ent}} = \ln N, \quad (25)$$

obtained when $\xi_n = N^{-1}$ for each n (maximally-entangled states).

Our explicit evaluation of the e-ph entanglement entropy is illustrated in Figs. 6 and 7, where it is depicted for $\phi_{dc} = 0.975\pi$ and two different initial bare-excitation quasimomenta ($k_0 = \pi/2, \pi/4$) and phonon frequencies ($\delta\omega/2\pi = 200$ MHz, 300 MHz). In particular, Fig. 6 illustrates that the growth of this entanglement entropy

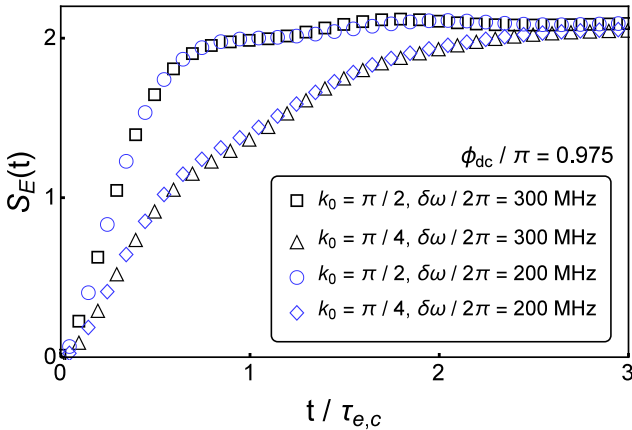


FIG. 7: (Color online) Short-time behavior of the e-ph entanglement entropy for $\phi_{dc} = 0.975\pi$ and different choices of values for k_0 and $\delta\omega$.

from zero at $t = 0$ starts with an abrupt increase on timescales of the order of a few $\tau_{e,c}$. This short-time behavior of the entropy is depicted separately in Fig. 7, from which we can infer that at short times $S_E(t)$ depends on k_0 , but is essentially independent of $\delta\omega$. The abrupt increase of $S_E(t)$ is followed by oscillations at later times. Those oscillations, which are much more pronounced for $k_0 = \pi/4$ than for $k_0 = \pi/2$, are another manifestation of the late-time recurrences, akin to those found in $n_{\text{ph}}(t)$ and $P_{k_0=\pi/2}(t)$ [recall Sec. IV A].

Another important feature of the e-ph entanglement entropy, which can be inferred from the obtained results, is that at times $t \approx (2 - 3) \tau_{e,c}$ – coinciding with the corresponding SP formation times τ_{sp} – this quantity indeed reaches values close to those characterizing maximally-entangled states [note that for $N = 9$, we have $S_{\text{max-ent}} = 2.197$]. For instance, the respective maximal values of $S_E(t)$ obtained for the above case of $k_0 = \pi/2$ are 2.141 for $\delta\omega/2\pi = 200$ MHz and 2.115 for 300 MHz. This is consistent with the results of an earlier study that reached the conclusion that typical SP ground states are essentially maximally entangled³⁴.

V. SUMMARY AND CONCLUSIONS

To summarize, in this work we explored the dynamics of small-polaron formation in the presence of two different mechanisms of nonlocal excitation-phonon interaction within the framework of an analog simulator. In this simulator, which is based on an array of coupled superconducting qubits (transmons or gatemon) and microwave resonators, the pseudospin degree of freedom of qubits plays the role of spinless-fermion excitation, while photons in the resonators mimic dispersionless phonons. By employing a numerically-exact approach – diagonalization of the effective system Hamiltonian combined with the Chebyshev-propagator method for computing its dynamics – we determined the formation time of small polarons that ensue from initially-prepared bare-excitation Bloch states following an excitation-phonon (qubit-resonator) interaction quench.

We analyzed how this important dynamical timescale depends on the initial bare-excitation quasimomentum and the effective coupling strength. We then further characterized the system dynamics by evaluating the excitation-phonon entanglement entropy and demonstrating its growth from zero (before the interaction quench) to values close to those inherent to maximally-entangled states. Finally, by computing the dynamical variances of the phonon position- and momentum quadratures we also demonstrated the non-Gaussian character of small-polaron states resulting from the quench, with a strong anti-squeezing in both quadratures.

The present work constitutes a systematic theoretical study of the quantum dynamics of small-polaron formation resulting from strongly momentum-dependent

excitation-phonon coupling. Such couplings, in their own right, are of utmost importance for understanding charge-transport mechanisms in several classes of electronic materials. The advanced measurement capabilities of the proposed superconducting analog simulator should allow an accurate verification of our quantitative predictions. To make contact with previous studies of the same phenomenon involving other types of polarons, we compared and contrasted our findings with those pertaining to the small-polaron formation dynamics in the presence of purely local (momentum-independent) Holstein-type excitation-phonon interaction^{20,21}. We found, for instance, that in the system at hand – where excitation-phonon coupling itself is strongly momentum-dependent – the small-polaron formation time shows a weaker dependence on the initial bare-excitation quasimomentum than in the Holstein-polaron case.

Several directions of future work can be envisioned. Firstly, the proposed simulator can be utilized for investigations of further nonequilibrium aspects of small-polaron physics, which have so far also been discussed only for Holstein-type excitation-phonon interaction^{48–51}. Examples of such aspects include the small-polaron dynamics in the presence of an external electric field⁴⁸, as well as the dynamics following a strong oscillatory pulse⁴⁹. Furthermore, while the proposed system serves as a simulator for a one-dimensional excitation-phonon model, the continuously-improving scalability of superconducting-qubit systems should allow one to fabricate – in not-too-distant future – a two-dimensional counterpart of this simulator. Such a system could be used for studying the effects of dimensionality on the formation of small-polaron-type quasiparticles; analogous effects have proven to be quite interesting in the case of Holstein polarons. Finally, a different type of qubit-resonator arrays – featuring effective XXZ -type coupling between qubits⁵² – would allow an investigation of intersite bipolarons⁵³, quasiparticles closely related to small polarons. Experimental realization of the proposed system is keenly anticipated.

Acknowledgments

V.M.S. acknowledges useful discussions with L. Tian during previous collaborations on related topics. In the initial stages of this project V.M.S. was supported by the SNSF. This work was supported in part by the Serbian Ministry of Science and Technological Development under grant numbers 171027 (V.M.S.) and ON 171031 (I.S.).

Appendix A: Symmetry-adapted basis and details of exact diagonalization

The Hilbert space of the coupled e-ph system is spanned by states $|n\rangle_e \otimes |\mathbf{m}\rangle_{\text{ph}}$, where $|n\rangle_e \equiv c_n^\dagger |0\rangle_e$ cor-

responds to the excitation localized at the site n , while

$$|\mathbf{m}\rangle_{\text{ph}} = \prod_{n=1}^{N \otimes} \frac{(b_n^\dagger)^{m_n}}{\sqrt{m_n!}} |0\rangle_{\text{ph}}, \quad (\text{A1})$$

where $\mathbf{m} \equiv (m_1, \dots, m_N)$ are the phonon occupation numbers at different sites. We restrict ourselves to the truncated phonon Hilbert space that includes states with the total number of phonons $m = \sum_{n=1}^N m_n$ not larger than M , where $0 \leq m_n \leq m$. Accordingly, the total Hilbert space of the system has the dimension $D = D_e \times D_{\text{ph}}$, where $D_e = N$ and $D_{\text{ph}} = (M + N)!/(M!N!)$.

The dimension of the Hamiltonian matrix to be diagonalized can be further reduced by exploiting the discrete translational symmetry of the system, whose mathematical expression is the commutation $[H_{\text{eff}}, K_{\text{tot}}] = 0$ of operators H_{eff} and K_{tot} . This permits diagonalization of H_{eff} in Hilbert-space sectors corresponding to the eigensubspaces of K_{tot} , where the dimension of each of those K -sectors of the total Hilbert space coincides with that of the truncated phonon space, i.e., $D_K = D_{\text{ph}}$. To this end, we utilize the symmetry-adapted basis

$$|K, \mathbf{m}\rangle = N^{-1/2} \sum_{n=1}^N e^{iKn} \mathcal{T}_n(|1\rangle_e \otimes |\mathbf{m}\rangle_{\text{ph}}), \quad (\text{A2})$$

with \mathcal{T}_n being the (discrete) translation operators whose action ought to comply with the periodic boundary conditions. The last equation can be recast as

$$|K, \mathbf{m}\rangle = N^{-1/2} \sum_{n=1}^N e^{iKn} |n\rangle_e \otimes \mathcal{T}_n^{\text{ph}} |\mathbf{m}\rangle_{\text{ph}}, \quad (\text{A3})$$

where the operators $\mathcal{T}_n^{\text{ph}}$ represent the action of discrete translations in the phonon Hilbert space. Note that, if $|\mathbf{m}\rangle_{\text{ph}}$ is defined by a set of occupation numbers

$$|\mathbf{m}\rangle_{\text{ph}} = |m_1, m_2, \dots, m_N\rangle_{\text{ph}}, \quad (\text{A4})$$

then $\mathcal{T}_n^{\text{ph}} |\mathbf{m}\rangle_{\text{ph}} \equiv |\mathcal{T}_n^{\text{ph}} \mathbf{m}\rangle$ is given by

$$|\mathcal{T}_n^{\text{ph}} \mathbf{m}\rangle = |m_{N-n+1}, m_{N-n+2}, \dots, m_{N-n}\rangle_{\text{ph}}. \quad (\text{A5})$$

In general, in terms of the original phonon occupation numbers, the r -th occupation number in $|\mathcal{T}_n^{\text{ph}} \mathbf{m}\rangle$ is given by $m_{s(r,n)}$, where the site index $s(r,n)$ is defined by

$$s(r,n) \equiv \begin{cases} N - n + r, & \text{for } r \leq n \\ r - n, & \text{for } r > n \end{cases}. \quad (\text{A6})$$

Regarding the ground-state calculations, we follow an established phonon Hilbert-space truncation procedure²³ whereby the system size (N) and the maximum number of phonons retained (M) are increased until the convergence for the ground-state energy and the phonon distribution is reached. Our adopted convergence criterion is that the relative error in the ground-state energy and the phonon distribution upon further increase of N and M is not larger than 10^{-4} . The adopted criterion is here satisfied for the system size $N = 9$ (with periodic boundary conditions) and requires the total of $M = 10$ phonons.

Appendix B: Matrix elements and expectation values

1. Derivation of the matrix elements of relevant observables

In what follows, we first derive the expressions for the expectation values of a generic observable with respect to the state $|\psi(t)\rangle$ of the system at time t . In view of our use of the symmetry-adapted basis [cf. Eq. (A2)], we do so by deriving the matrix elements of the same observables in that basis. We then specialize to the relevant observables for our present work – the total phonon (photon) number [defined by Eq. (18)], as well as the variances of the phonon position and momentum quadratures corresponding to an arbitrary site [defined by Eq. (20)].

We start from the decomposition of the state $|\psi(t)\rangle$ in the symmetry-adapted basis [defined in Eq. (A2) above]

$$|\psi(t)\rangle = \sum_{\mathbf{m}} C_{\mathbf{m}}^K(t) |K, \mathbf{m}\rangle, \quad (\text{B1})$$

where the expansion coefficients $C_{\mathbf{m}}^K(t)$ can be obtained through our computation of the state evolution. For an arbitrary observable A we then have

$$\langle \psi(t) | A | \psi(t) \rangle = \sum_{\mathbf{m}, \mathbf{m}'} C_{\mathbf{m}'}^{K*}(t) C_{\mathbf{m}}^K(t) \langle K, \mathbf{m}' | A | K, \mathbf{m} \rangle, \quad (\text{B2})$$

which – with already known expansion coefficients – leaves us with the task of calculating the matrix elements $\langle K, \mathbf{m}' | A | K, \mathbf{m} \rangle$ for the relevant observables.

Assuming – as is the case for our relevant observables – that A depends only on phonon operators, it is straightforward to show, using Eq. (A3), that

$$\langle K, \mathbf{m}' | A | K, \mathbf{m} \rangle = \frac{1}{N} \sum_{n=1}^N \langle \mathcal{T}_n^{\text{ph}} \mathbf{m}' | A | \mathcal{T}_n^{\text{ph}} \mathbf{m} \rangle, \quad (\text{B3})$$

where in deriving this last result we made use of the fact that ${}_e \langle n' | n \rangle_e = \delta_{nn'}$. Before embarking on further derivations it is useful to note that $\langle \mathcal{T}_n^{\text{ph}} \mathbf{m}' | \mathcal{T}_n^{\text{ph}} \mathbf{m} \rangle$ is independent of n and equals 1 if the two sets of phonon occupation numbers – \mathbf{m} and \mathbf{m}' – are completely the same, otherwise it evaluates to zero. In other words,

$$\langle \mathcal{T}_n^{\text{ph}} \mathbf{m}' | \mathcal{T}_n^{\text{ph}} \mathbf{m} \rangle = \delta_{\mathbf{m}, \mathbf{m}'}. \quad (\text{B4})$$

In the simplest case, for $A = a_r^\dagger a_r$, we first note that

$$a_r^\dagger a_r | \mathcal{T}_n^{\text{ph}} \mathbf{m} \rangle = m_{s(r,n)} | \mathcal{T}_n^{\text{ph}} \mathbf{m} \rangle, \quad (\text{B5})$$

where $s(i, n)$ is defined by Eq. (A6). By inserting the last result into Eq. (B3) and making use of Eq. (B4) we then easily obtain that

$$\langle K, \mathbf{m}' | a_r^\dagger a_r | K, \mathbf{m} \rangle = \frac{\delta_{\mathbf{m}, \mathbf{m}'}}{N} \sum_{n=1}^N m_n. \quad (\text{B6})$$

where – owing to the discrete translational symmetry of the system – the RHS of the last equation does not explicitly depend on r . [In writing the last equation, we made use of the fact that $\sum_{n=1}^N m_{s(r,n)} \equiv \sum_{n=1}^N m_n$]. By extension, for $A = \sum_{r=1}^N a_r^\dagger a_r$ (total photon number), we get

$$\langle K, \mathbf{m}' | \sum_{r=1}^N a_r^\dagger a_r | K, \mathbf{m} \rangle = \delta_{\mathbf{m}, \mathbf{m}'} \sum_{n=1}^N m_n. \quad (\text{B7})$$

Upon inserting the last result into the general Eq. (B2), we obtain the desired expectation value

$$\langle \psi(t) | \sum_{r=1}^N a_r^\dagger a_r | \psi(t) \rangle = \sum_{n, \mathbf{m}} m_n |C_{\mathbf{m}}^K(t)|^2. \quad (\text{B8})$$

For $A = a_r$, we first notice that

$$a_r | \mathcal{T}_n^{\text{ph}} \mathbf{m} \rangle = \sqrt{m_{s(r,n)}} | \mathcal{T}_n^{\text{ph}} \mathbf{m}_{(r,-1)} \rangle. \quad (\text{B9})$$

where $| \mathcal{T}_n^{\text{ph}} \mathbf{m}_{(r,-1)} \rangle$ is the vector obtained by changing the r -th occupation number in $| \mathcal{T}_n^{\text{ph}} \mathbf{m} \rangle$ from $m_{s(r,n)}$ to $m_{s(r,n)} - 1$. This implies that

$$\langle \mathcal{T}_n^{\text{ph}} \mathbf{m}' | a_r | \mathcal{T}_n^{\text{ph}} \mathbf{m} \rangle = \sqrt{m_{s(r,n)}} \quad (\text{B10})$$

provided that the two sets (\mathbf{m} and \mathbf{m}') have the same occupation numbers except at site $s(r, n)$ where $m'_{s(r,n)}$ should be equal to $m_{s(r,n)} - 1$; otherwise, $\langle \mathcal{T}_n^{\text{ph}} \mathbf{m}' | a_r | \mathcal{T}_n^{\text{ph}} \mathbf{m} \rangle = 0$. The desired matrix element $\langle K, \mathbf{m}' | a_r | K, \mathbf{m} \rangle$ is obtained by combining Eq. (B10) and the general result in Eq. (B3).

In an analogous fashion, for $A = a_r^\dagger$ we obtain

$$\langle \mathcal{T}_n^{\text{ph}} \mathbf{m}' | a_r^\dagger | \mathcal{T}_n^{\text{ph}} \mathbf{m} \rangle = \sqrt{m_{s(r,n)} + 1} \quad (\text{B11})$$

if the two sets (\mathbf{m} and \mathbf{m}') have the same occupation numbers except at site $s(r, n)$ where $m'_{s(r,n)}$ should be equal to $m_{s(r,n)} + 1$; otherwise, $\langle \mathcal{T}_n^{\text{ph}} \mathbf{m}' | a_r^\dagger | \mathcal{T}_n^{\text{ph}} \mathbf{m} \rangle = 0$. The matrix element $\langle K, \mathbf{m}' | a_r^\dagger | K, \mathbf{m} \rangle$ sought for is easily obtained by inserting the expression in Eq. (B11) into the general Eq. (B3).

By combining the derived expressions for $\langle K, \mathbf{m}' | a_r | K, \mathbf{m} \rangle$ and $\langle K, \mathbf{m}' | a_r^\dagger | K, \mathbf{m} \rangle$, we can easily obtain the desired results for $\langle K, \mathbf{m}' | x_r | K, \mathbf{m} \rangle$ and $\langle K, \mathbf{m}' | p_r | K, \mathbf{m} \rangle$.

When $A = x_r^2 = (a_r^\dagger + a_r)^2/2$ or $A = p_r^2 = -(a_r^\dagger - a_r)^2/2$, we first note that

$$x_r^2 \equiv \frac{1}{2} [2a_r^\dagger a_r + 1 + (a_r^\dagger)^2 + a_r^2], \quad (\text{B12})$$

$$p_r^2 \equiv \frac{1}{2} [2a_r^\dagger a_r + 1 - (a_r^\dagger)^2 - a_r^2]. \quad (\text{B13})$$

Repeating the above procedure, to compute the desired matrix elements $\langle K, \mathbf{m}' | (a_r^\dagger)^2 | K, \mathbf{m} \rangle$ and $\langle K, \mathbf{m}' | a_r^2 | K, \mathbf{m} \rangle$, we have to first determine

$\langle \mathcal{T}_n^{\text{ph}} \mathbf{m}' | (a_r^\dagger)^2 | \mathcal{T}_n^{\text{ph}} \mathbf{m} \rangle$ and $\langle \mathcal{T}_n^{\text{ph}} \mathbf{m}' | a_r^2 | \mathcal{T}_n^{\text{ph}} \mathbf{m} \rangle$. It is straightforward to show that, for instance,

$$\langle \mathcal{T}_n^{\text{ph}} \mathbf{m}' | (a_r^\dagger)^2 | \mathcal{T}_n^{\text{ph}} \mathbf{m} \rangle = \sqrt{[m_{s(r,n)} + 1][m_{s(r,n)} + 2]} \quad (\text{B14})$$

provided that the two sets (\mathbf{m} and \mathbf{m}') have the same occupation numbers except at site $s(r,n)$ where $m'_{s(r,n)}$ should be equal to $m_{s(r,n)} + 2$; otherwise, $\langle K, \mathbf{m}' | (a_r^\dagger)^2 | K, \mathbf{m} \rangle = 0$. Similarly, we have that

$$\langle \mathcal{T}_n^{\text{ph}} \mathbf{m}' | a_r^2 | \mathcal{T}_n^{\text{ph}} \mathbf{m} \rangle = \sqrt{m_{s(r,n)}[m_{s(r,n)} - 1]} \quad (\text{B15})$$

if the two sets (\mathbf{m} and \mathbf{m}') have the same occupation numbers except at site $s(r,n)$ where $m'_{s(r,n)}$ should be equal to $m_{s(r,n)} - 2$; otherwise, $\langle \mathcal{T}_n^{\text{ph}} \mathbf{m}' | a_r^2 | \mathcal{T}_n^{\text{ph}} \mathbf{m} \rangle = 0$.

With the aid of the expressions for the matrix elements obtained thus far, and using the general expression in Eq. (B2) with the coefficients $C_{\mathbf{m}}^K(t)$ obtained from the computation of the system dynamics, one can straightforwardly obtain the variances $S_x(t)$ and $S_p(t)$ of the position and momentum quadratures [cf. Eq. (20)].

2. Derivation of the matrix elements of the reduced density matrix

In what follows, we derive expressions for the matrix elements of the reduced density matrix assuming that the system under consideration evolves starting from a bare-excitation Bloch state with quasimomentum k_0 at $t = 0$.

We make use of our standard symmetry-adapted basis [cf. Eq. (A3)] for $K = k_0$:

$$|K = k_0, \mathbf{m}\rangle = N^{-1/2} \sum_{n=1}^N e^{ik_0 n} |n\rangle_e \otimes \mathcal{T}_n^{\text{ph}} |\mathbf{m}\rangle_{\text{ph}}. \quad (\text{B16})$$

and start by expanding the state $|\psi(t)\rangle$ of the system at time t with respect to this basis:

$$|\psi(t)\rangle = \sum_{\mathbf{m}} C_{\mathbf{m}}^{k_0}(t) |k_0, \mathbf{m}\rangle, \quad (\text{B17})$$

The density matrix of our composite (bipartite) e-ph system at time t is given by Eq. (21) and – using the expansion in Eq. (B17) – can be expressed as

$$\rho_{\text{e-ph}}(t) = \sum_{\mathbf{m}, \mathbf{m}'} C_{\mathbf{m}'}^{k_0*}(t) C_{\mathbf{m}}^{k_0}(t) |k_0, \mathbf{m}\rangle \langle k_0, \mathbf{m}'|. \quad (\text{B18})$$

By now making use of Eq. (A3), i.e., its special case for $K = k_0$, we further obtain:

$$\begin{aligned} \rho_{\text{e-ph}}(t) &= N^{-1} \sum_{\mathbf{m}, \mathbf{m}'} \sum_{n, n'=1}^N e^{ik_0(n-n')} C_{\mathbf{m}'}^{k_0*}(t) C_{\mathbf{m}}^{k_0}(t) \\ &\times |n\rangle \langle n'| \otimes |\mathcal{T}_n^{\text{ph}} \mathbf{m}\rangle \langle \mathcal{T}_{n'}^{\text{ph}} \mathbf{m}'|. \end{aligned} \quad (\text{B19})$$

The reduced excitation density matrix is obtained by tracing the last density matrix over the phonon basis [cf. Eq. (22)]. Let \mathbf{m}'' be the dummy index for the phonon basis states, i.e., the set of all phonon occupation-number configurations. Then we have

$$\rho_e(t) = \sum_{\mathbf{m}''} \langle \mathbf{m}'' | \rho_{\text{e-ph}}(t) | \mathbf{m}'' \rangle, \quad (\text{B20})$$

which, by inserting $\rho_{\text{e-ph}}(t)$ from Eq. (B19), becomes

$$\begin{aligned} \rho_e(t) &= N^{-1} \sum_{\mathbf{m}, \mathbf{m}', \mathbf{m}''} \sum_{n, n'=1}^N e^{ik_0(n-n')} C_{\mathbf{m}'}^{k_0*}(t) C_{\mathbf{m}}^{k_0}(t) \\ &\times \langle \mathcal{T}_{n'}^{\text{ph}} \mathbf{m}' | \mathbf{m}'' \rangle \langle \mathbf{m}'' | \mathcal{T}_n^{\text{ph}} \mathbf{m} \rangle |n\rangle \langle n'|. \end{aligned} \quad (\text{B21})$$

We now note that

$$\sum_{\mathbf{m}''} \langle \mathcal{T}_{n'}^{\text{ph}} \mathbf{m}' | \mathbf{m}'' \rangle \langle \mathbf{m}'' | \mathcal{T}_n^{\text{ph}} \mathbf{m} \rangle = \langle \mathcal{T}_{n'}^{\text{ph}} \mathbf{m}' | \mathcal{T}_n^{\text{ph}} \mathbf{m} \rangle, \quad (\text{B22})$$

where we made use of the completeness relation in the phonon Hilbert space

$$\sum_{\mathbf{m}''} |\mathbf{m}''\rangle \langle \mathbf{m}''| = \mathbb{1}. \quad (\text{B23})$$

Using the result in Eq. (B22), the expression for $\rho_e(t)$ in Eq. (B21) now simplifies to

$$\begin{aligned} \rho_e(t) &= N^{-1} \sum_{\mathbf{m}, \mathbf{m}'} \sum_{n, n'=1}^N e^{ik_0(n-n')} C_{\mathbf{m}'}^{k_0*}(t) C_{\mathbf{m}}^{k_0}(t) \\ &\times \langle \mathcal{T}_{n'}^{\text{ph}} \mathbf{m}' | \mathcal{T}_n^{\text{ph}} \mathbf{m} \rangle |n\rangle \langle n'|. \end{aligned} \quad (\text{B24})$$

From the last equation we readily read off the final expression for the matrix elements of the reduced excitation density matrix:

$$\begin{aligned} (\rho_e)_{nn'}(t) &= N^{-1} e^{ik_0(n-n')} \sum_{\mathbf{m}, \mathbf{m}'} C_{\mathbf{m}'}^{k_0*}(t) C_{\mathbf{m}}^{k_0}(t) \\ &\times \langle \mathbf{m}' | \mathcal{T}_{n-n'}^{\text{ph}} \mathbf{m} \rangle, \end{aligned} \quad (\text{B25})$$

where we made use of the fact that $\langle \mathcal{T}_{n'}^{\text{ph}} \mathbf{m}' | \mathcal{T}_n^{\text{ph}} \mathbf{m} \rangle \equiv \langle \mathbf{m}' | \mathcal{T}_{n-n'}^{\text{ph}} \mathbf{m} \rangle$. It is also useful to note that the final result in Eq. (B25) can more succinctly be recast as

$$(\rho_e)_{nn'}(t) = N^{-1} e^{ik_0(n-n')} \langle \psi(t) | \mathcal{T}_{n-n'}^{\text{ph}} | \psi(t) \rangle. \quad (\text{B26})$$

In order to evaluate the matrix element $\langle \mathbf{m}' | \mathcal{T}_{n-n'}^{\text{ph}} \mathbf{m} \rangle$, it is useful to recall Eqs. (A5) and (A6). Note that $\langle \mathcal{T}_{n'}^{\text{ph}} \mathbf{m}' | \mathcal{T}_n^{\text{ph}} \mathbf{m} \rangle = 1$ if all the corresponding phonon occupation numbers in $|\mathcal{T}_n^{\text{ph}} \mathbf{m}\rangle$ and $|\mathcal{T}_{n'}^{\text{ph}} \mathbf{m}'\rangle$ are the same, otherwise this matrix element evaluates to zero.

Appendix C: Chebyshev-propagator method (CPM) for dynamics

In the following, we briefly recapitulate the essential aspects of the computational technique utilized in

the present work – the Chebyshev-propagator method (CPM)³⁹ – followed by some basic details of our concrete implementation thereof. A more detailed introduction into the CPM is provided in Ref. 40.

1. Basics of the CPM

For a system described by the Hamiltonian H , the time-evolution operator $U(t + \delta t, t) = U(\delta t) = e^{-iH\delta t}$ can be expanded in a finite series of N_C Chebyshev polynomials of the first-kind $T_p(x) = \cos(p \arccos x)$ ^{39,40}:

$$U(\delta t) = e^{-ib\delta t} \left[c_0(a\delta t) + 2 \sum_{p=1}^{N_C} c_p(a\delta t) T_p(\tilde{H}) \right]. \quad (\text{C1})$$

Here $\tilde{H} = (H - b)/a$ is a rescaled Hamiltonian of the system, where E_{\min} (E_{\max}) is the minimal (maximal) eigenvalue of H , $b = (E_{\max} + E_{\min})/2$, and $a = (E_{\max} - E_{\min} + \epsilon)/2$, with $\epsilon = \alpha_c(E_{\max} - E_{\min})$ being introduced to ensure that the rescaled spectrum lies well inside $[-1, 1]$. The expansion coefficients are given by

$$c_p(a\delta t) = \int_{-1}^1 \frac{T_p(x) e^{-ixt}}{\pi \sqrt{1-x^2}} dx = (-i)^p J_p(a\delta t), \quad (\text{C2})$$

where $J_p(a\delta t)$ is the p -th order Bessel function of the first kind. In cases where the system Hamiltonian does not depend explicitly on time, these expansion coefficients also depend only on the time step δt (but not explicitly on time t), thus it is sufficient to compute them only once.

The recurrence relations for the Chebyshev polynomials³⁹ can be used to simplify the computation of the state evolution $|\psi(t + \delta t)\rangle = U(\delta t)|\psi(t)\rangle$ from one point on a time grid to the next one. The problem is effectively reduced to the iterative evaluation of vectors $|v_p\rangle \equiv T_p(\tilde{H})|\psi(t)\rangle$ using the recursive relation

$$|v_{p+1}\rangle = \tilde{H}|v_p\rangle - |v_{p-1}\rangle, \quad (\text{C3})$$

where $|v_0\rangle = \psi(t)$ and $|v_1\rangle = \tilde{H}|v_0\rangle$. Evolving the state vector $|\psi(t)\rangle$ from one time step to the next one requires N_C matrix-vector multiplications of a given complex vector with a sparse Hamiltonian matrix, a step that for the system evolution from $t = 0$ to $t = t_f$ has to be performed $t_f/\delta t$ times.

Given that the CPM requires only the knowledge of two extremal eigenvalues of the system Hamiltonian, it is convenient to combine it with Lanczos-type diagonalization for sparse matrices⁴⁶. The CPM has by now proven to be superior to other direct or iterative integration schemes, in terms of both computational cost and accuracy⁵⁴.

2. Implementation details and numerical consistency checks

The results obtained for the system dynamics in this work were based on calculations performed for a system with $N = 9$ qubits, with up to $M = 20$ phonons in the truncated phonon Hilbert space. Thus, the resulting maximal dimension of the truncated phonon Hilbert space (as discussed in Sec. A of this Appendix, this is also the dimension of any K -sector of the full Hilbert space) was $D \approx 10^7$ and to make the storage of the nonzero matrix elements possible we used the sparse-matrix form. Reaching the numerical convergence in our dynamics calculations typically required us to use between $N_C = 9$ and $N_C = 14$ Chebyshev polynomials in the expansion given by Eq. (C1). Besides, the smallest time step required for numerical convergence was $\delta t = 0.05 \tau_{e,c}$, i.e., up to 20 time steps were used within the period that corresponds to the physically meaningful (excitation-hopping) timescale $\tau_{e,c} \approx 0.44$ ns. Our runs included those with the total evolution times t_f as large as $100 \tau_{e,c}$, i.e., with up to 2,000 such time steps. In our calculations, ϵ was kept at the fixed value of 10^{-3} (cf. Sec. C1).

We carried out our CPM-based dynamics calculations on an 8-core, 3.5 GHz Intel Xeon CPU E5-1620 machine, with a total of 32 GB of main memory. The runs that were required to obtain all the results presented in this paper consumed less than 250 CPU hours.

The results were checked for consistency whenever it was possible. In particular, testing for unitarity turned out to be a good measure of convergence of the CPM. Namely, at each iteration step the norm of the evolving state vector was calculated and any deviation from unity larger than 10^{-4} was considered a surefire sign that a higher precision (i.e., either a shorter time step or a larger N_C) is needed. Despite the fact that we maintained this unitarity margin of error to be much lower than 10^{-4} throughout our calculations, this was not always sufficient and additional convergence tests – performed by increasing computational precision and confirming the stability of the results – were carried out.

As another internal consistency check, we used the mathematical relation between the expectation values of x_r^2 , p_r^2 , and the phonon-number operator $a_r^\dagger a_r$ that stems from the identity $x_r^2 + p_r^2 = 2a_r^\dagger a_r + 1$. This relation was satisfied by our data at 10^{-7} precision, which is a highly nontrivial test as the expectation values of x_r^2 and p_r^2 on one hand, and that of $a_r^\dagger a_r$ on the other, were evaluated by completely different and mutually independent means.

- ¹ For an introduction, see U. Vool and M. Devoret, *Int. J. Circ. Theor. Appl.* **45**, 897 (2017).
- ² For an up-to-date review, see G. Wendin, *Rep. Prog. Phys.* **80**, 106001 (2017).
- ³ I. M. Georgescu, S. Ashhab, and F. Nori, *Rev. Mod. Phys.* **86**, 153 (2014).
- ⁴ J. Koch, T. M. Yu, J. Gambetta, A. A. Houck, D. I. Schuster, J. Majer, A. Blais, M. H. Devoret, S. M. Girvin, and R. J. Schoelkopf, *Phys. Rev. A* **76**, 042319 (2007).
- ⁵ For an introduction, see S. M. Girvin, in *Lecture Notes on Strong Light-Matter Coupling: from Atoms to Solid-State Systems* (World Scientific, Singapore, 2013).
- ⁶ A. A. Houck, H. E. Türeci, and J. Koch, *Nature Phys.* **8**, 292 (2012).
- ⁷ G. S. Paraoanu, J. Low. Temp. Phys. **175**, 633 (2014).
- ⁸ For a recent review, see L. Lamata, A. Parra-Rodriguez, M. Sanz, and E. Solano, *Advances in Physics: X* **3**, 1457981 (2018).
- ⁹ F. Mei, V. M. Stojanović, I. Siddiqi, and L. Tian, *Phys. Rev. B* **88**, 224502 (2013).
- ¹⁰ V. M. Stojanović, M. Vanević, E. Demler, and L. Tian, *Phys. Rev. B* **89**, 144508 (2014).
- ¹¹ S. Mostame, J. Huh, C. Kreisbeck, A. J. Kerman, T. Fujita, A. Eisfeld, and A. Aspuru-Guzik, *Quant. Info. Proc.* **16**, 44 (2017).
- ¹² V. M. Stojanović, T. Shi, C. Bruder, and J. I. Cirac, *Phys. Rev. Lett.* **109**, 250501 (2012).
- ¹³ A. Mezzacapo, J. Casanova, L. Lamata, and E. Solano, *Phys. Rev. Lett.* **109**, 200501 (2012).
- ¹⁴ F. Herrera and R. V. Krems, *Phys. Rev. A* **84**, 051401(R) (2011).
- ¹⁵ F. Herrera, K. W. Madison, R. V. Krems, and M. Berciu, *Phys. Rev. Lett.* **110**, 223002 (2013).
- ¹⁶ J. P. Hague and C. McCormick, *Phys. Rev. Lett.* **109**, 223001 (2012).
- ¹⁷ J. Ranninger, in *Proc. Int. School of Physics “E. Fermi”, Course CLXI*, edited by G. Iadonisi, J. Ranninger, and G. De Filippis (IOS Press, Amsterdam, 2006), pp. 1–25.
- ¹⁸ A. S. Alexandrov and J. T. Devreese, *Advances in Polaron Physics* (Springer-Verlag, Berlin, 2010).
- ¹⁹ S. Engelsberg and J. R. Schrieffer, *Phys. Rev.* **131**, 993 (1963).
- ²⁰ L.-C. Ku and S. A. Trugman, *Phys. Rev. B* **75**, 014307 (2007).
- ²¹ H. Fehske, G. Wellein, and A. R. Bishop, *Phys. Rev. B* **83**, 075104 (2011).
- ²² T. Holstein, *Ann. Phys. (N.Y.)* **8**, 343 (1959).
- ²³ G. Wellein and H. Fehske, *Phys. Rev. B* **56**, 4513 (1997).
- ²⁴ G. Wellein and H. Fehske, *Phys. Rev. B* **58**, 6208 (1998).
- ²⁵ N.-H. Ge, C. M. Wong, R. L. Lingle Jr., J. D. McNeill, K. J. Gaffney, and C. B. Harris, *Science* **279**, 202 (1998); S. Tomimoto, H. Nansei, S. Saito, T. Suemoto, J. Takeda, and S. Kurita, *Phys. Rev. Lett.* **81**, 417 (1998); S. L. Dexheimer, A. D. Van Pelt, J. A. Brozik, and B. I. Swanson, *ibid.* **84**, 4425 (2000); A. Sugita, T. Saito, H. Kano, M. Yamashita, and T. Kobayashi, *ibid.* **86**, 2158 (2001).
- ²⁶ S. Ciuchi and S. Fratini, *Phys. Rev. Lett.* **106**, 166403 (2011); N. Vukmirović, C. Bruder, and V. M. Stojanović, *ibid.* **109**, 126407 (2012); K. Hannewald, V. M. Stojanović, and P. A. Bobbert, *J. Phys: Condens. Matter* **16**, 2023 (2004).
- ²⁷ K. Hannewald, V. M. Stojanović, J. M. T. Schellekens, P. A. Bobbert, G. Kresse, and J. Hafner, *Phys. Rev. B* **69**, 075211 (2004).
- ²⁸ See, e.g., L. M. Woods and G. D. Mahan, *Phys. Rev. B* **61**, 10651 (2000); V. M. Stojanović, N. Vukmirović, and C. Bruder, *ibid.* **82**, 165410 (2010); N. Vukmirović, V. M. Stojanović, and M. Vanević, *ibid.* **81**, 041408(R) (2010).
- ²⁹ O. Rösch and O. Gunnarsson, *Phys. Rev. Lett.* **92**, 146403 (2004).
- ³⁰ C. Slezak, A. Macridin, G. A. Sawatzky, M. Jarrell, and T. A. Maier, *Phys. Rev. B* **73**, 205122 (2006).
- ³¹ V. M. Stojanović, P. A. Bobbert, and M. A. J. Michels, *Phys. Rev. B* **69**, 144302 (2004).
- ³² M. Zoli, *Phys. Rev. B* **70**, 184301 (2004).
- ³³ S. Barišić, J. Labbé, and J. Friedel, *Phys. Rev. Lett.* **25**, 919 (1970).
- ³⁴ V. M. Stojanović and M. Vanević, *Phys. Rev. B* **78**, 214301 (2008).
- ³⁵ B. Gerlach and H. Löwen, *Rev. Mod. Phys.* **63**, 63 (1991).
- ³⁶ T. W. Larsen, F. Kuemmeth, T. S. Jespersen, P. Krogstrup, J. Nygård, and C. M. Marcus, *Phys. Rev. Lett.* **115**, 127001 (2015).
- ³⁷ L. Casparis, T. W. Larsen, M. S. Olsen, F. Kuemmeth, P. Krogstrup, J. Nygård, K. D. Petersson, and C. M. Marcus, *Phys. Rev. Lett.* **116**, 150505 (2016).
- ³⁸ A. Kringhøj, L. Casparis, M. Hell, T. W. Larsen, F. Kuemmeth, M. Leijnse, K. Flensberg, P. Krogstrup, J. Nygård, K. D. Petersson, and C. M. Marcus, *Phys. Rev. B* **97**, 060508(R) (2018).
- ³⁹ H. Tal-Ezer and R. Kosloff, *J. Chem. Phys.* **81**, 3967 (1984).
- ⁴⁰ For a review, see R. Kosloff, *Annu. Rev. Phys. Chem.* **45**, 145 (1994).
- ⁴¹ P. Coleman, *Introduction to Many-Body Physics* (Cambridge University Press, Cambridge, UK, 2015).
- ⁴² For other types of tunable couplers, see M. R. Geller, E. Donate, Y. Chen, C. Neill, P. Roushan, and J. M. Martinis, *Phys. Rev. A* **92**, 012320 (2015).
- ⁴³ T. P. Orlando and K. A. Delin, *Introduction to Applied Superconductivity* (Addison-Wesley, Reading, MA, 1991).
- ⁴⁴ M. Hohenadler, *Phys. Rev. Lett.* **117**, 206404 (2016).
- ⁴⁵ V. M. Stojanović, C. Wu, W. V. Liu, and S. Das Sarma, *Phys. Rev. Lett.* **101**, 125301 (2008).
- ⁴⁶ J. K. Cullum and R. A. Willoughby, *Lanczos Algorithms for Large Symmetric Eigenvalue Computations* (Birkhäuser, Boston, 1985).
- ⁴⁷ B. R. Johnson, M. D. Reed, A. A. Houck, D. I. Schuster, Lev S. Bishop, E. Ginossar, J. M. Gambetta, L. DiCarlo, L. Frunzio, S. M. Girvin, and R. J. Schoelkopf, *Nat. Phys.* **6**, 663 (2010).
- ⁴⁸ L. Vidmar, J. Bonča, M. Mierzejewski, P. Prelovšek, and S. A. Trugman, *Phys. Rev. B* **83**, 134301 (2011).
- ⁴⁹ D. Golež, J. Bonča, L. Vidmar, and S. A. Trugman, *Phys. Rev. Lett.* **109**, 236402 (2012).
- ⁵⁰ S. Sayyad and M. Eckstein, *Phys. Rev. B* **91**, 104301 (2015).
- ⁵¹ F. Dorfner, L. Vidmar, C. Brockt, E. Jeckelmann, and F. Heidrich-Meisner, *Phys. Rev. B* **91**, 104302 (2015).
- ⁵² R. Heule, C. Bruder, D. Burgarth, and V. M. Stojanović, *Eur. Phys. J. D* **63**, 41 (2011).
- ⁵³ J. Ranninger, in *Proc. Int. School of Physics “E. Fermi”*,

Course CLXI, edited by G. Iadonisi, J. Ranninger, and G. De Filippis (IOS Press, Amsterdam, 2006), pp. 327–347.

⁵⁴ C. Leforestier *et al.*, J. Comp. Phys. **94**, 59 (1991).